Transparent conducting oxide films for thin film silicon photovoltaics

W. Beyer, J. Hüpkes and H. Stiebig

IEF-5 Photovoltaik, Forschungszentrum Jülich GmbH, D-52425 Jülich, Germany

Abstract

Requirements for application of transparent conducting oxide (TCO) films in thin film silicon solar cells are reviewed with a focus on sputtered Al doped zinc oxide films. TCO films are employed as a front contact and as part of a highly reflective back contact so that the silicon absorber layer is embedded by TCO films.. Optoelectronic properties of TCO layers and their influence on the solar cell performance are discussed. In addition, recent results on stability issues of such films, solar cells and solar modules are presented.

Keywords: zinc oxide, stability, solar cell, solar module, amorphous silicon, microcrystalline silicon

1. Introduction

Silicon thin film solar cells are presently produced at a level of 80 – 100 MW per year which is about 5 % of the world solar cell production. They have an efficiency of typically 5 to 7 % and are predominantly based on amorphous silicon as the absorber material. In recent time, great efforts are undertaken worldwide to develop tandem solar cells with amorphous and microcrystalline Si absorber layers. For this type of solar cells, module efficiencies > 10 % appear feasible. In particular in Germany, the up-scaling of thin film Si solar cell production is in progress, as the installation of production capacitance of more than 200 MW per year has been announced. It is hoped that by mass production of thin film silicon solar cells, the price of photovoltaics based electricity can be reduced significantly.

Besides the silicon absorber layers, transparent conducting oxide (TCO) films are also important components of thin film Si solar cells. Such highly conducting TCO layers are commonly used as contact layers of pin solar cell structures [1, 2, 3, 4]. Since the lateral conductance of doped p/n silicon layers is not sufficient to prevent resistive losses over typical distances in the range of 1 cm, a TCO front layer is used to avoid a high series resistance [1]. Furthermore, front contact TCO layers serve the purpose of (i) an effective coupling of light into the solar cell by refractive index matching and (ii) an efficient light trapping by scattering of light into the solar cell at rough TCO/silicon interface. Also at the rear contact of the solar cell, TCO layers are applied. Purposes are current extraction similar as the TCO front contact [4, 5], or the improvement of optical properties of the metal back contact. A direct contact of the metal (usually silver or aluminium) with silicon is known to cause optical absorption losses [6]. Furthermore, the long term stability of the ZnO/Ag rear contact is superior to the Ag layer in direct contact with silicon [3, 7]. Fig. 1 shows the structure of a typical a-Si/μc-Si tandem cell. The silicon thin film diodes are embedded between two TCO layers. For the choice of proper TCO, several criteria are of importance:

(i) high transparency in the range of the solar spectrum,

(ii) high conductivity ,

(iii) high carrier mobility,

(iv) well suited refractive index for coupling of light into the silicon absorber material,

(v) grown or patterned TCO films with surface texture for optimum light scattering,

(vi) high chemical stability of the bulk material and of the contact to silicon,

(vii) non-toxic and sustainable materials,

(viii) low cost.

Three types of TCOs have been applied so far (or are in progress of application) in commercial thin film silicon solar cells: tin oxide (SnO_2), indium-tin oxide (ITO) and ZnO. Of these, ITO is certainly the most expensive TCO as it contains a seizable fraction of indium,

which is a metal of low abundancy on earth and its price is increasing strongly in recent time. On the other hand, both tin and zinc oxide are highly abundant and are considered environmentally harmless. The most common TCO used in present amorphous silicon solar cells is SnO_2 (F doped) where a high quality product is the Asahi U substrate [8]. In recent time, TCO materials based on ZnO are developed [9, 10]. Aim of this article is to review requirements of TCO layers for achieving high solar cell efficiencies. Some recent results on stability issues of TCO layers in thin film Si solar cells will also be discussed.

2. Preparation methods of TCO layers

Various methods have been applied for TCO preparation. The methods involve spray pyrolysis, vapour and liquid phase or sol-gel deposition, pulsed laser deposition and sputtering. Tin oxide often is prepared by chemical vapour deposition (CVD) using $SnCl_4$ precursor gas [8, 11, 12]. In case of zinc oxide preparation for silicon thin film solar cells, CVD processes (using, e.g., $Zn(C_2H_5)_2$ as a precursor gas) or sputter deposition are applied [9, 10]. The applied substrate (process) temperatures differ quite significantly. E.g., for zinc oxide prepared by CVD, temperatures near 150°C are applied [5, 9] while for ZnO prepared by sputtering, the typical process temperatures are near 300°C. For the present study, the ZnO:Al films were prepared by radio frequency sputtering from ceramic $ZnO:Al_2O_3$ (99:1wt%) and undoped ZnO targets. The pressure was kept constant at about 0.1 Pa. More details concerning the deposition conditions and systems used are given elsewhere [10, 13].

3. TCO Properties

3.1. Conductivity

High n-type conductivities can be obtained for both ZnO and SnO_2 by doping. In case of ZnO, this is commonly achieved by adding aluminium, gallium or boron, although doping by fluorine has also been reported. Tin oxide is most often doped by fluorine, but also by gallium or boron. For both types of TCO highest conductivities range from 10^3 to $5x10^3$ $(\Omega cm)^{-1}$. Mobilities in these highly doped materials range from near 30 cm^2/Vs to 60 cm^2/Vs [8, 11, 12, 14, 15]. It has been shown that higher mobilities can be achieved at lower doping levels [14 - 17]. Recent work [18] has identified also hydrogen as a possible n-type dopant. This is quite interesting, since hydrogen is an ubiquitous impurity in these materials forming (e.g.) OH bonds. For the present type of solar cell, a p-type TCO would be highly appreciated for the front contact to achieve a good ohmic contact to the p-doped silicon layer of the solar cell. However, so far no highly conducting p-type TCO has been realized [19].

3.2. Optical absorption

The application in terrestrial solar cells requires bandgaps exceeding 3 eV and low concentration of defects. Undoped Zinc oxide has a bandgap of 3.4 eV and undoped SnO_2 of 3.6 eV [15]. Figure 2 shows optical transmission and absorption spectra of two differently doped ZnO:Al films. The films are highly transparent in the visible range. High doping levels lead to a shift of free carrier absorption into the near IR range, resulting in a significant absorption also in the active spectral range of silicon solar cells. Note that high doping levels also affect the optical constants significantly leading, e.g. for highly doped ZnO:Al to a widening of the bandgap.

3.3. Light scattering properties

In order to provide effective coupling of light into thin film solar cells, rough TCO-silicon interfaces are commonly used in silicon thin film technology. Scattering of light at these rough interfaces, together with a significantly higher refractive index of the Si material, as compared to the TCO materials, cause the solar cells to act as effective light traps increasing the solar cell efficiency and saving costs, as the solar cell can be made thinner. In order to obtain rough TCO material, different strategies have been applied, namely the growth of rough TCO layers, the growth of smooth TCO layers on textured glass or the post-deposition texturing. Note, however, that post-deposition texturing is generally applied only for zinc oxide, which is easy to etch by diluted acid. Most common in present-day a-Si solar cell technology is the application of tin oxide films which have a texture from growth. In case of zinc oxide films, both as-grown surface-textured films as well as a post-deposition surface-texturing are applied. Post-deposition texturing has some advantage, as the optimization of the light scattering is partially separated from the electronic properties. Theoretical and experimental studies have shown that the surface topography is quite important for an effective light trapping within solar cells [9, 17, 20 - 24].

Fig. 3 shows scanning electron microscope (SEM) images of an (a) as deposited and (b) etched ZnO:Al film. Sputtered ZnO:Al is initially smooth. By a wet-chemical etching step in diluted hydrochloric acid (typically 0.5% HCl) a texturing of the ZnO:Al surface is obtained. With increasing etching time the roughness of the surface increases from 7 nm (initial value) to 162 nm (optimized conditions).

The quantum efficiency and total cell absorption (1-R, R = reflectivity) of µc-Si:H p-i-n cells prepared on smooth and texture etched ZnO:Al substrates are shown in fig. 4. The quantum efficiency of the cell with rough interfaces exceeds the sensitivity of the cell with flat interfaces in the whole spectral range. The cell prepared on the optimized texture etched ZnO:Al substrate exhibits an increase in short-circuit current density by more than 7 mA/cm^2,

due to an improved light in-coupling and enhanced long wavelength absorption. The current of the thin-film solar cells increases from 16.3 mA/cm^2 for a flat cell assembly to 23.4 mA/cm^2 for a solar cell structure with rough interfaces with an i-layer thickness of 1 µm. In addition, the interference fringes characteristic of a flat film disappear due to destruction of phase correlation between the different reflected beams by the rough interfaces. However, fig. 4 also demonstrates an intrinsic problem of light trapping: The optical losses in the non-active layers of the cell are also enhanced by light trapping [25]. These absorption losses are given by the difference between QE and (1-R) in fig. 4. This difference increases strongly with longer wavelengths (in the near infrared (NIR)). The reason for this is the free carrier absorption in the TCO layer, which is much stronger than absorption of silicon for light of longer wavelengths. The absorption within the TCO is strongly enhanced by internal light trapping, as a part of the light is multiply reflected within the solar cell. For this reason, a high NIR transmission of front TCO is very important to minimize optical losses. Consequently, a reduced charge carrier density and thus a reduced doping level is reasonable.

4. Stability issues

Three stability effects in relation to TCO are of major concern in thin film technology, the stability of the TCO against hydrogen plasma, the stability of the TCO-silicon contact and the stability of the TCO itself against annealing or reaction with environmental substances.

4.1. Stability against hydrogen plasma

This stability effect is of particular importance when microcrystalline Si films deposited by plasma CVD from silane at high hydrogen dilution on top of TCO material. For tin oxide (and

indium tin oxide), a rapid reduction with the formation of metallic tin and a consequent increase in optical absorption has been reported [26, 27]. Such a reduction has not been observed for ZnO films [26, 27]. As an explanation it has been speculated that also zinc oxide is reduced by hydrogen and that the resulting metallic zinc evaporates [26] or that the formation of surface Zn-H or ZnOH species may lead to a passivation of the surface towards reduction by H plasma [27]. In order to study the nature of this difference, we applied a deuterium plasma of 10 and 30 min, respectively, on ZnO and SnO_2 films at T = 200°C. The results of SIMS depth profiling of deuterium is shown in fig. 5.

It is seen that deuterium penetrates intrinsic ZnO (fig. 5 b) at rather low concentration of about 10^{19} cm^{-3} and shows error-function type profiles typical for an in-diffusion process. Such behaviour has been noted by others [28]. In case of the SnO_2 layer, deuterium penetrates at a much higher concentration level of more than 10^{20} cm^{-3} and the profiles show a plateau-like (i.e. non error-function) shape. Very likely, this plateau zone indicates the zone of reaction where SnO_2 has been reduced (partially) to tin. Thus, the difference in the behaviour of ZnO and SnO_2 in hydrogen plasma seems to arise basically by two effects, a higher hydrogen penetration level and a lower bulk diffusion in SnO_2 as compared to ZnO. Both effects combined lead, apparently, to a high enough local concentration of hydrogen (deuterium) in SnO_2 so that the reaction $SnO_2 + 2\ H_2 \Rightarrow Sn + 2\ H_2O$ proceeds. The difference in deuterium penetration may arise from different hydrogen surface desorption effects. The different H diffusion in the bulk is also reflected by our (preliminary) results for H interdiffusion. Here, we find at 450°C an at least a factor of 10 lower H diffusion coefficient in SnO_2 than in ZnO.

4.2. Interface reaction with silicon

Interface reactions of tin and zinc oxides with silicon have been demonstrated using various techniques [29, 30]. It is quite clear that in a narrow thickness range the oxides are reduced to tin and zinc, respectively with the formation of silicon oxide at the same time [29]. As long as the resulting silicon dioxide interlayer is thin enough, electrons may tunnel through it so the performance of a solar cell may only be slightly affected. Thicker growth of silicon dioxide requires oxygen diffusion or silicon diffusion to the respective reaction surfaces. This diffusion process is expected to be small in the temperature range the solar cells are operated as long as the silicon dioxide has a compact structure. At high temperatures ($T > 400°C$) such interface reactions have been found to lead to a reduction of the complete tin oxide layer [30].

4.3. Stability against atmospheric influences and out diffusion of components

Although thin film solar cells are provided with an encapsulation, in a lifetime of a solar cell of exceeding 20 years the out- and in-diffusion of atoms and molecules could be a matter of concern. The long term stability of tin oxide and zinc oxide based TCO can be estimated from the stability of corresponding minerals in nature. Tin oxide is known to be the dominant tin bearing mineral and occurs in nature to a large fraction in sedimentary deposits containing small grains of the mineral [31]. This demonstrates a very high stability against atmospheric influences. Zinc oxide, on the other hand, occurs in nature only in a limited number of deposits while most zinc is mined in the form of sulphides, carbonates and hydrocarbonates [31]. From this, a lower stability of zinc oxide against environmental influences can be concluded. On the other hand it is known that the high stability of metallic zinc in atmospheric environment is largely based on the formation of a thin coverage by zinc oxides and zinc carbonates. We note that the rather easy surface texturing of zinc oxide using highly diluted hydrochloric acid demonstrates a low stability of the material in diluted acids.

An important factor for the long term stability is the microstructure of the material which determines what size of molecules (like molecular hydrogen, oxygen, water) can diffuse out and in from the material at ambient or solar cell operation temperatures. In order to characterize network openings, we have developed a characterization method involving the out-diffusion of implanted rare gas atoms of different size [32]. Fig. 6 shows He and Ne effusion spectra for a ZnO single crystal and for ZnO thin films deposited by sputtering of a ceramic target (1 wt% Al_2O_3) at the substrate temperatures 60 and 290°C. Plotted is the effusion rate of He and Ne as a function of temperature (heating rate was 20 K/min). It is seen that He effuses for all samples near 500-600°C, neon is seen to effuse for the ZnO films above 600°C while no Ne effusion is visible for the ZnO single crystal up to 1050°C. Since rare gases do not form bonds to the host material, doorway diffusion processes are likely [33]. For such processes, a strong dependence of the diffusion energy on the size of the diffusing atoms (or molecules) is expected in agreement with the present data. Note that from literature data, the atomic diameter of He is about 0.2 nm, of Ne (and H_2) about 2.5 nm and of O_2, H_2O, CO and CO_2 more than 3 nm [34]. For diffusion in a homogeneous medium, the diffusion coefficient can be estimated from the temperature T_M of the effusion maximum using the formula [32].

$$D/E_D = d^2 \beta / k \pi T_M^2 \qquad \text{(eqn. (1))}$$

with d the film thickness, β the heating rate and k the Boltzmann constant. For He diffusion in the ZnO crystal, we get from the data of fig. 6 E_D = 1.55 eV assuming D to follow and Arrhenius law with the theoretical diffusion prefactor of $D_0 \sim 10^{-3}$ cm^2s^{-1} [32]. Similar He diffusion parameters have been found for crystalline Si. Since no Ne effusion is observed up to 1050°C in the ZnO crystal, the diffusion energy must exceed 2.5 eV. For the ZnO films,

some Ne effusion is visible at high temperatures and the He effusion peak is much broader and (for T_S = 290°C) shifted considerably to lower temperature. From previous work on amorphous or microcrystalline Si [35] it is known that shifts to lower T can arise from the presence of interconnected voids while shifts to higher T can be attributed to the presence of isolated voids. Thus, the present results suggest the presence of interconnected voids in particular for high T_S material.

In fig. 7 the mean temperature T* of He effusion is plotted as a function of the substrate temperature T_S. T* is defined by the temperature when half of the implanted He is evolved. It is seen that up to T_S= 200°C, T* is similar to the ZnO crystal while it is almost 100°C lower in T_S > 200°C material (which is the material used in our solar cells). It is tempting to associate this downshift with relatively open grain boundaries. Such grain boundaries are known to exist from TEM pictures. If He and Ne atoms effuse from ZnO grains into open grain boundaries, the effective material thickness d in eqn. 1 is much smaller than the actual film thickness and the downshift of both Ne and He peaks can be explained. In any case, the results demonstrate that our sputtered ZnO is (apart from the grain boundaries) a highly compact material with little in and out-diffusion of atoms or molecules with sizes > Ne (H_2) up to 1000°C. In $T_S \leq$ 200°C material grain boundaries seem to have no effect on He effusion, in agreement with a long range diffusion of hydrogen in this type of material (not shown here).

4.4. Long term stability of thin-film silicon solar cells and modules

The long term stability of non-encapsulated thin-film silicon cells and modules is an important issue of their development and application. Costs and effort for module encapsulation strongly depends on the stability of non-encapsulated devices. In order to investigate the long-term stability of solar cells and solar modules, damp heat testing is

commonly applied. Here, solar cells are exposed to harsh conditions (85 % humidity, 85 °C) for many hours.

As mentioned above, a high reflective back-contact is essential to enable multiple reflections within the solar cell. Using only an Ag-layer as a rear contact leads to a surprising result. The FF of diodes with an Ag back contact drops down after 20 - 100 h of exposure time due to adhesion problems of the silver layer on the silicon. The silver layer starts to peel off and the series resistance increases. With increasing testing time (>10h) also the short circuit current decreases and the dark I/V behavior differs from the initial state (top of fig. 8). However, a contrary behavior is observed for the red response of μc-Si:H solar cells (bottom of fig. 8) measured under low illumination intensity. In the long wavelength region the quantum efficiency (QE) increases with time and reaches values which even exceed the QE of samples with a ZnO/Ag back contact. For λ = 750 nm the QE increseses by more than 50%. This result demonstrates that a simple Ag back contact leads to strong optical losses, since Ag grows in islands [6]. When the metal layer locally peels off, the optical losses disappear. If a ZnO layer is introduced between the silicon and silver layer, the adhesion is highly improved and the optical losses are also significantly reduced. After 2000 h of damp heat testing no significant degradation is observed for thin-film silicon solar cells based on a-Si:H and μc-Si:H single pin structures employing both types of TCOs (SnO and ZnO) and a-Si:H/μc-Si:H tandem cells when a ZnO/Ag-back contact is applied..

While for solar cells the TCO/Ag back contact is optimized with respect to a high reflectivity and good stability, for thin-film silicon modules further aspects have to be considered. Laser patterning of the ZnO/metal layer stack and high throughput for the deposition of the back contact, which can be achieved by sputtering, define additional requirements for the TCO layer. An optimized thickness has to be considered since, with increasing Ag layer thickness, the stability of the back contact increases and the probability for a flake-free laser scribing process (and shunt-free module) decreases. Furthermore, the study has shown that the stability

of solar cells with sputtered metal layer increases with sputtering temperature [7]. Therefore, special design rules have to be considered to realize modules with high long term stability [36]. For a non-encapsulated microcrystalline silicon thin-film module prepared at Jülich, the fill factor decreases less than 3% after more than 1500 h damp heat testing. Fig. 9 shows the relative module parameters: module efficiency (η) and fill factor (FF) (left) and open circuit voltage (Voc) and short circuit current (I_{sc}) (right) as a function of the exposure time. The parameters are normalized by their initial values. The initial efficiency of the investigated μc-Si:H module was 8.32%. In this case the ZnO and Ag back contact layer stack was optimized in respect to a high reflectivity, flake free line scribing process by laser ablation and high long term stability. This result indicates that it is possible to achieve inherent stability of non-encapsulated thin-film silicon modules using thin-film silicon layers embedded between ZnO-layers.

5. Conclusions

It is demonstrated that the incorporation of TCO materials in the silicon thin film solar cell technology is a highly challenging effort, requiring in particular further material and solar cell research. The present results and achievements demonstrate that both SnO_2 and ZnO materials are suitable for the use in thin film silicon solar cells. Both materials have similar optical and electrical properties, but the chemistry is quite different. SnO_2 is highly stable against environmental substances as well as acids and bases but rather unstable against hydrogen plasma. ZnO is little affected by H plasma but quite unstable in acids. The latter property, however, bears the advantage that an easy after-deposition texturing is possible by wet etching. Thus, light coupling into thin film solar cells can be optimized. If thin film silicon

solar cells can be developed to contribute significantly to the world solar cell production, any improvement of TCO materials used can be of an enormous economic impact.

Acknowledgements

The authors with to thank U. Breuer (ZCH, FZJ) for the SIMS measurements, A. Doumit, W. Hilgers, D. Lennartz, W. Reetz, H. Siekmann and Ch. Zahren for technical assistance and M. Berginski, A. Gordijn, S. Haas for fruitful discussions.

References

[1] D.E. Carlson, C.R. Wronski, in: Amorphous Silicon, topics in Applied Physics Vol. 36, edited by M.H. Brodsky (Springer, Berlin 1979) 287-329.

[2] J. Müller, B. Rech, J. Springer, M. Vanecek, Solar Energy 77 (2004) 917.

[3] H. Stiebig, F. Siebke, W. Beyer, C. Beneking, B. Rech, H. Wagner, Solar Energy Materials and Solar Cells 48 (1997) 351.

[4] A. Shah, P. Torres, R. Tscharner, N. Wyrsch, H. Keppner, Sience 285 (1999) 692.

[5] U. Kroll, J. Meier, S. Benagli, T. Roschek, J. Spitznagel, A. Huegli, D. Borello, M. Mohr, O. Kluth, D. Zimin, G. Monteduro, J. Springer, G. Androutsopoulos, C. Ellert, W. Stein, G. Buechel, A. Zindl, A. Buechel, D. Koch-Ospelt, Proc. 21st European Photovoltaic Solar Energy Conference, Dresden (2006) 1546.

[6] H. Stiebig, A. Kreisel, K. Winz, N. Schultz, C. Beneking, Th. Eickhoff, H. Wagner, M. Meer, Proceedings of the 1st World Conference on Photovoltaic Energy Conversion, Hawaii (1994) 603.

[7] H. Stiebig, W. Reetz, C. Zahren, T. Repmann, B. Rech, Proc. IEEE World Conference on Photovoltaic energy conversion, Hawaii, USA (2006) 1521.

[8] K. Sato, Y. Gotoh, Y. Wakayama, Y. Haya shi, K. Atachi, H. Nishimura, Rep. Res. Lab. Asahi Glass Co, Ltd., 42 (1992) 129.

[9] S. Faÿ, L. Feitknecht, R. Schlüchter, U. Kroll, E. Vallat-Sauvain, A. Shah, Solar Energy Materials and Solar Cells, Volume 90 (2006) 2960.

[10] O. Kluth, G. Schöpe, J. Hüpkes, C. Agashe, J. Müller, B. Rech, Thin Solid Films 442 (2003) 80.

[11] A. E. Rakhshani, Y. Makdisi, H. A. Ramazaniyan, J. Appl. Phys. **83** , (1998) 1049.

[12] B. Kuhn, D. Le Bellac, B. Rech, J. Hüpkes, G. Schöpe, Proc. 19th European photovoltaic solar energy conference and exhibition, Dresden, Germany (2006) 1733.

[13] B. Rech, T. Repmann, M.N. van den Donker, M. Berginski, T. Kilper, J. Hüpkes, S. Calnan, H. Stiebig, S. Wieder, Thin Solid Films 511 – 512 (2006) 548.

[14] C. Agashe, O. Kluth, J. Hüpkes, U. Zastrow, B. Rech, J. Appl. Phys. 95 (2004) 1911

[15] K. Ellmer, J. Phys. D **34**, (2001) 3097.

[16] T. Minami, H. Sato, K. Ohashi, T. Tomofuji, S. Tarata, J. Cryst. Growth, 117, (1992) 370.

[17] M. Berginski, J. Hüpkes, M. Schulte, G. Schöpe, H. Stiebig, B. Rech, M. Wuttig, J. Appl. Phys. 101 (2007) 074903.

[18] G.C. van de Walle, Phys. Rev. Letters 85 (2000) 1012.

[19] D. C. Look, Semicond. Sci. Technol. **20** (2005) S55.

[20] H. Schade, Z.E. Smith, Journal of Applied Optics, 24 (1985) 3221.

[21] M. Zeman, R.A.C.M.M. van Sway, M. Zuiddam, J.W. Metselaar, Material Research Society Symposium Proceedings **557** (1999) 725.

[22] J. Krč, F. Smole, M. Topič, Progress in Photovoltaics: Research and Applications, 11(2003) 429.

[23] S. Hegedus, R. Kaplan, Progress in Photovoltaics: Research and Applications, 10 (2002) 257.

[24] H. Stiebig, N. Senoussaoui, C. Zahren, C. Haase, J. Müller, Progress in Photovoltaics: Research and Applications 14 (2006) 13.

[25] T. Brammer, W. Reetz, N. Senoussaoui, O. Vetterl, O. Kluth, B. Rech, H. Stiebig, H. Wagner , Solar Energy Materials & Solar Cells 74 (2002) 469.

[26] T. Minami, H. Sato, H. Nanto, S.Takata, Thin Solid Films 176 (1989) 277.

[27] S. Major, S. Kumar, M. Bhatnagar, K.L. Chopra, Appl. Phys. Lett 49 (1986) 394.

[28] N. Nickel, Phys. Rev. B 73, 19, (2006) 195204.

[29] H. Fujiwara, M. Kondo, A. Matsuda, J. Appl. Phys. 93 (2003) 2400.

[30] F. Edelman, R. Brener, C. Cytermann, M. Eizenberg , R. Weil, W. Beyer, Appl. Phys. Lett. 67 (1995) 389.

[31] Klockmanns, Lehrbuch der Mineralogie (Ferdinand Enke Verlag, Stuttgart, Germany, 1978).

[32] W. Beyer, Phys Stat Sol (c)1 (2004) 1144.

[33] O.L. Anderson, D.A. Stuart, J. Am. Ceram. Society 37 (1954) 573.

[34] Landolt-Börnstein, Atom- und Molekularphysik I (Springer Verlag, Berlin, Germany, 1950) 325.

[35] W. Beyer, R. Carius, U. Zastrow, J. Non-Cryst. Solids 352 (2006) 1402.

[36] S. Haas, T. Repmann, W. Psyk, C. Zahren, B. Rech, H. Stiebig, Proc. 19th European photovoltaic solar energy conference and exhibition, Dresden, Germany (2006) 1707.

Captions

Fig. 1. Sketch of a-Si:H/µc-Si:H tandem solar cell structure. The silicon based pin/pin absorber layers are sandwiched by two TCO layers.

Fig. 2. Optical transmission and absorption spectra of ZnO:Al films with different doping levels. The doping concentration and carrier density are given in the graph.

Fig. 3. SEM micrographs of RF sputter deposited ZnO:Al films directly (a) after deposition and (b) after optimized etching step.

Fig. 4. Measured quantum efficiency (QE) and cell absorption (1-R) of µc-Si:H solar cells using smooth (solid) and texture etched (dotted).ZnO:Al front contact, as shown in fig. 3: The short circuit current densities of the cells deposited on smooth and textured substrates are 16.3mA/cm^2 and 23.4mA/cm^2, respectively.

Fig. 5. SIMS depth profiles of deuterium in (a) SnO_2:F and (b) ZnO after deuterium plasma treatment at T =200°C.

Fig. 6. Effusion rate dN/dt versus temperature T of implanted He and Ne in ZnO crystal (top) and in ZnO:Al films deposited by sputtering at T_S = 290°C (middle) and 60°C (bottom).

Fig. 7. Mean temperature T* of He effusion as a function of substrate temperature T_S of ZnO:Al films grown by sputtering.

Fig. 8. Dark I/V characteristics (top) and quantum efficiency (bottom) of µc-Si:H diodes with an Ag back contact, deposited on aluminum-doped zinc oxide for different exposure times.

Fig. 9. Relative solar cell parameters as a function of damp heat exposure time t for a µc-Si:H module with an initial efficiency of 8.32 %.

Fig. 1

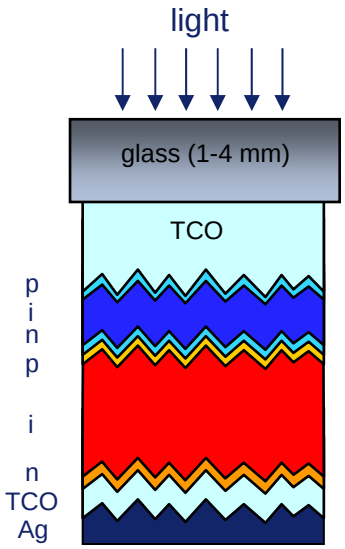
light
glass (1-4 mm)
TCO
p
i
n
p
i
n
TCO
Ag

Fig. 2

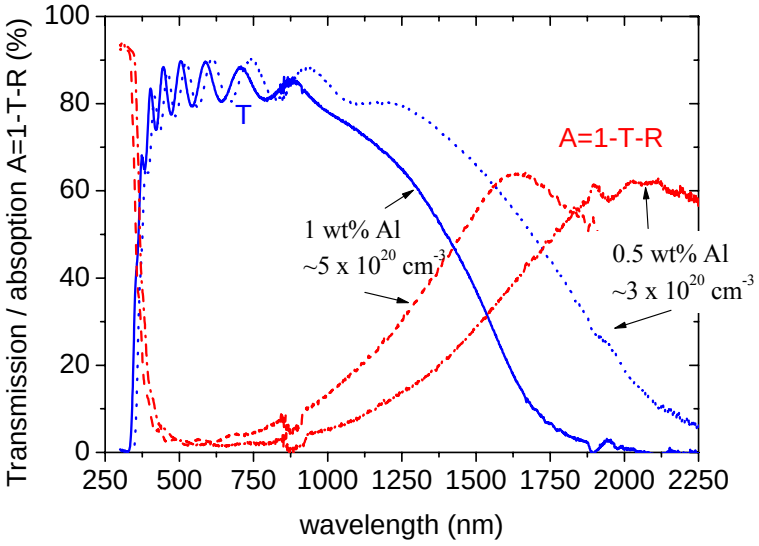
Transmission / absoption A=1-T-R (%)
wavelength (nm)
T
A=1-T-R
1 wt% Al
~5 x 10^20 cm^-3
0.5 wt% Al
~3 x 10^20 cm^-3
0
20
40
60
80
100
250
500
750
1000
1250
1500
1750
2000
2250

Fig. 3

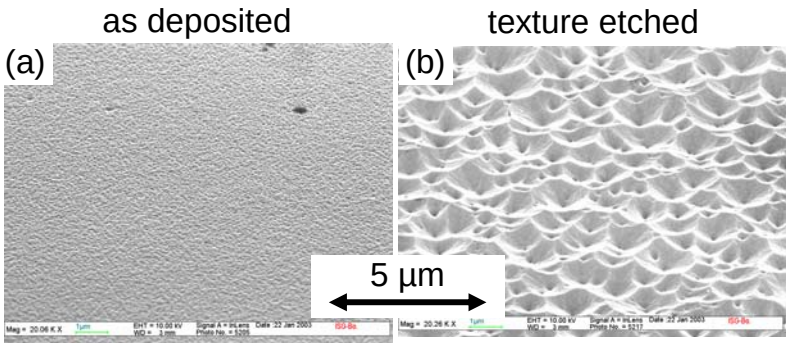
as deposited
texture etched
(a)
(b)
5 µm

Fig. 4

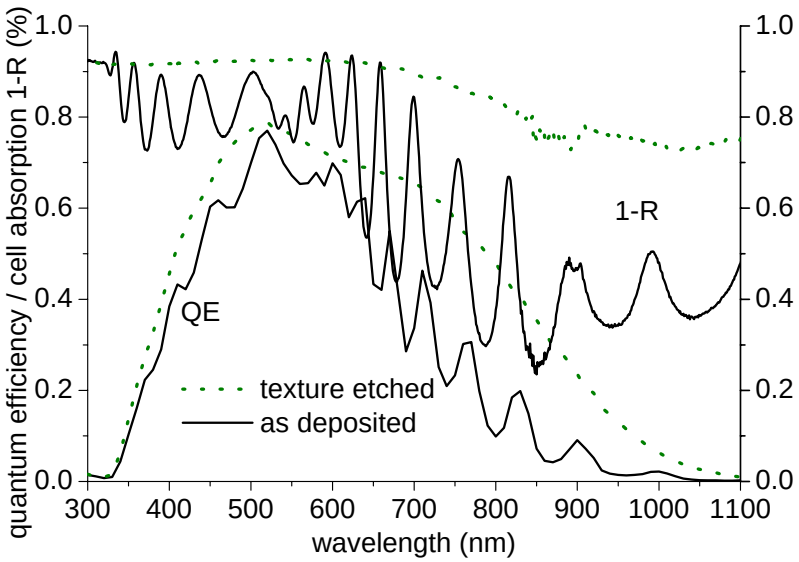
quantum efficiency / cell absorption 1-R (%)
wavelength (nm)
1-R
QE
texture etched
as deposited
0.0
0.2
0.4
0.6
0.8
1.0
300
400
500
600
700
800
900
1000
1100

Fig. 5

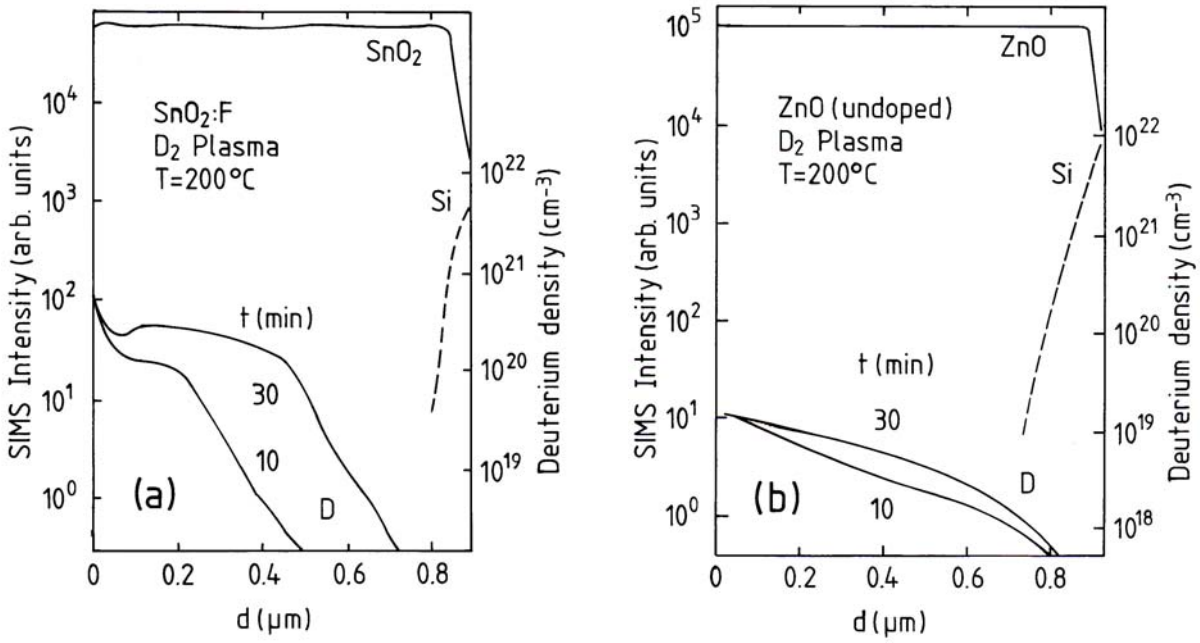
SnO2
SnO2:F
D2 Plasma
T=200°C
Si
t (min)
30
10
D
(a)
SIMS Intensity (arb. units)
Deuterium density (cm-3)
d (μm)
ZnO
ZnO (undoped)
D2 Plasma
T=200°C
Si
t (min)
30
10
D
(b)
SIMS Intensity (arb. units)
Deuterium density (cm-3)
d (μm)

Fig. 6

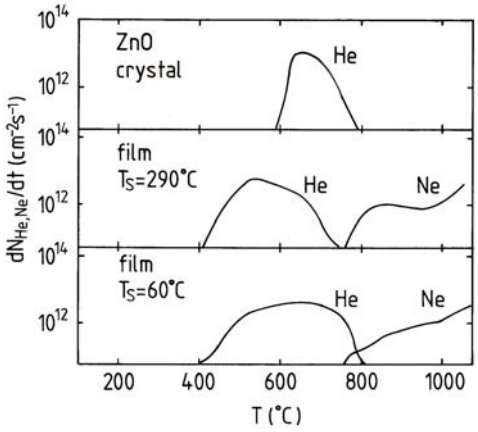
ZnO
crystal
He
film
T_S=290°C
He
Ne
film
T_S=60°C
He
Ne
10^{14}
10^{12}
$dN_{He,Ne}/dt$ ($cm^{-2}s^{-1}$)
200
400
600
800
1000
T (°C)

Fig. 7

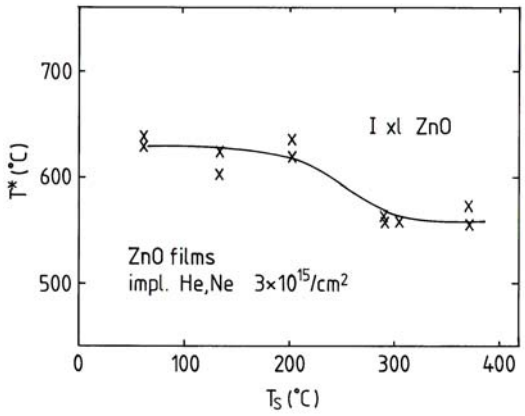
I xl ZnO
ZnO films
impl. He,Ne 3×10^{15}/cm^2
700
600
500
T* (°C)
0
100
200
300
400
T_S (°C)

Fig. 8

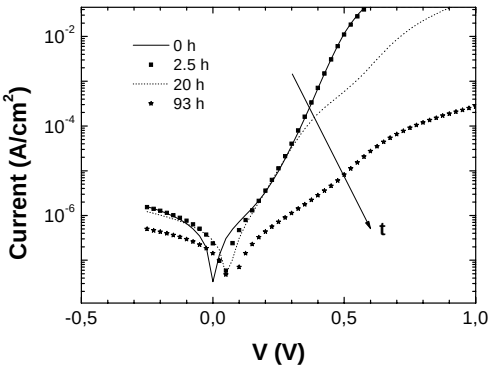
Current (A/cm^2)
10^{-2}
10^{-4}
10^{-6}
0 h
2.5 h
20 h
93 h
t
-0,5
0,0
0,5
1,0
V (V)

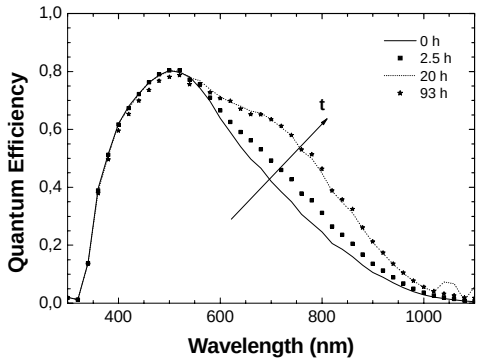
Quantum Efficiency
1,0
0,8
0,6
0,4
0,2
0,0
0 h
2.5 h
20 h
93 h
t
400
600
800
1000
Wavelength (nm)

Fig. 9

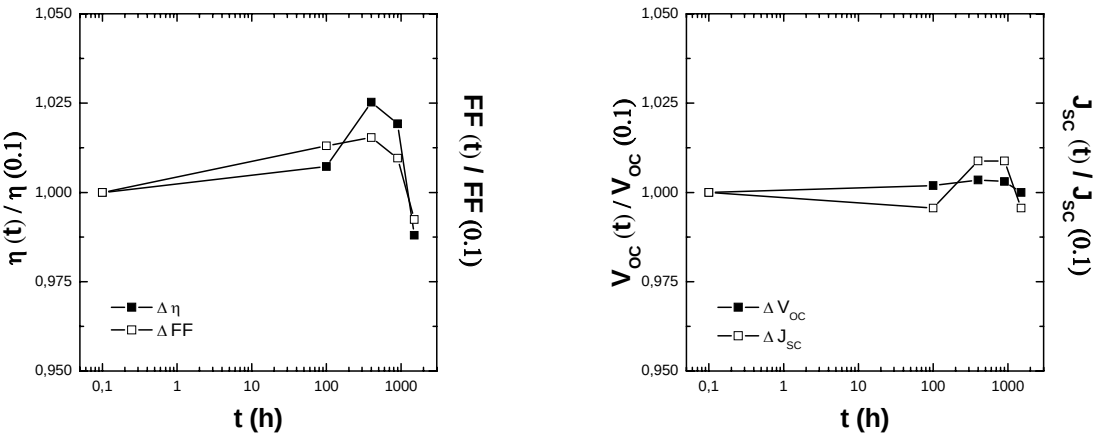
1,050
1,025
1,000
0,975
0,950
0,1
1
10
100
1000
t (h)
η (t) / η (0.1)
FF (t) / FF (0.1)
Δ η
Δ FF
V_oc (t) / V_oc (0.1)
J_sc (t) / J_sc (0.1)
Δ V_oc
Δ J_sc